1-14-2003

Electronic structure of ErAs(100)

Takashi Komesu
University of Nebraska-Lincoln, tkomesu2@unl.edu

Hae-Kyung Jeong
University of Nebraska-Lincoln, hjeong@unl.edu

Jaewu Choi
University of Nebraska-Lincoln, jchoi@ece.eng.wayne.edu

C.N. Borca
University of Nebraska-Lincoln

Peter A. Dowben
University of Nebraska-Lincoln, pdowben@unl.edu

See next page for additional authors

Electronic structure of ErAs(100)

Takashi Komesu, Hae-Kyung Jeong, Jaewu Choi, C. N. Borca, and P. A. Dowben
Department of Physics and Astronomy and the Center for Materials Research and Analysis, University of Nebraska-Lincoln, Lincoln, Nebraska 68588-0111

A. G. Petukhov
Center for Computational Materials Science, Naval Research Laboratory, Washington, DC 20375 and Physics Department, South Dakota School of Mines and Technology, Rapid City, South Dakota 57701-3995

B. D. Schultz and C. J. Palmstrøm
Department of Chemical Engineering and Material Science, University of Minnesota, Minneapolis, Minnesota 55455
(Received 28 June 2002; revised manuscript received 4 September 2002; published 14 January 2003)

The experimental band structure of the rare-earth pnictide erbium arsenide (ErAs), grown epitaxially on GaAs(100), has been mapped out using photoelectron spectroscopy and inverse photoemission spectroscopy. The electronic structure is dominated by bulk bands qualitatively consistent with the calculated band structure. A number of additional nondispersing $4f$ multiplet levels can be identified in the valence-band structure as well as at least one surface resonance band. From symmetry selection rules, photoemission provides strong evidence that the Δ_5 (or e) symmetry bands are a consequence of hybridization between Er and As, while the Δ_1 (or a_1) symmetry bands have possible contributions from nonbonding or antibonding states from Er (and/or As).

DOI: 10.1103/PhysRevB.67.035104 PACS number(s): 71.20.−b, 79.60.−i, 71.70.Ch

INTRODUCTION

Erbium arsenide (ErAs) is one of a class of rare-earth pnictides that have been the subject of much discussion regarding the band structure[1–10] because of the ''coupled'' magnetic and electronic properties. As magnetic materials, these materials are dominated by the strong exchange coupling between the relatively large local moments of $4f$ and valence and conduction electrons near the Fermi level (E_F) as well as exhibit strong wave vector dependent exchange splitting.[1–3] Both ferromagnetic and antiferromagnetic ordering are known,[11–13] with the nitrides typically exhibiting ferromagnetic ordering while the rare-earth arsenides and phosphides adopt antiferromagnetic ordering. With the coupling between the large $4f$ moments mediated by the valence and conduction electrons near E_F, clearly the magnetic properties are very sensitive to the band structure. While strong wave-vector exchange splitting is known in pure gadolinium,[14,15] with the rare-earth pnictides, the oscillator strength of the bands shifts from a rare earth to a pnictide with changing wave vector,[1–3] so that there are complications, additional to the expected contributions of band symmetry, short-range moment ordering, and spin-orbit coupling in determining the wave-vector-dependent exchange splitting.

Band structure is also the key to understanding the details of the spin-dependent tunneling through ErAs quantum wells.[16–18] Indeed the symmetry of the valence-band states in the vicinity of the Γ point of the bulk band structure is believed to play a key role. In general, the tunneling between a magnetic metal and a semiconductor is also expected to depend strongly upon band symmetries.[19–21]

Unfortunately, there is very little experimental data on the band structure of the rare-earth pnictides. Of the photoemission and inverse photoemission undertaken on this class of materials,[22–25] there are very few experimental band mappings.[24,25] In the previous experimental band structure studies of ErAs(100) (Ref. 24) some comparison with theory is possible, but much of the bulk band structure was not explored. In this paper, we detail some aspects of the experimental bulk band structure of the group-V rare-earth pnictide compound ErAs(100). This is made possible by the development of techniques for growing crystalline films of ErAs(100) on GaAs(100).[26]

EXPERIMENT

Several epitaxial crystalline thin films of ErAs(100) grown on GaAs(100) were created by molecular-beam epitaxy as described elsewhere,[26] and then capped with a thick As overlayer to prevent oxidation. The samples were then introduced into the separate ultra high vacuum (UHV) systems for angle-resolved photoemission or angle-resolved inverse photoemission, and the base pressure was maintained in the low 10^{-10} Torr range. The sample surfaces were cleaned in ultrahigh vacuum by Ar^+-ion sputtering and annealing to around 500 K to remove oxygen contamination and excess arsenic. The surfaces were found to be free of both oxygen and carbon using shallow core-level photoemission. With careful annealing of the sample, ErAs(100), the stoichiometric surface of ErAs was prepared. Both the low-energy electron-diffraction (LEED) pattern, as well as in situ scanning tunneling microscopy images of the ErAs(100) ultra thin films during the growth process, are consistent with the C_{4v} surface point group symmetry of the NaCl crystal structure, as described elsewhere[26] and indicated in Fig. 1. Angle-resolved x ray photoemission spectroscopy (XPS) measurements taken after the removal of the As capping layer provide further evidence of a compositionally uniform and stoichiometric ErAs thin film (the normalized Er/As

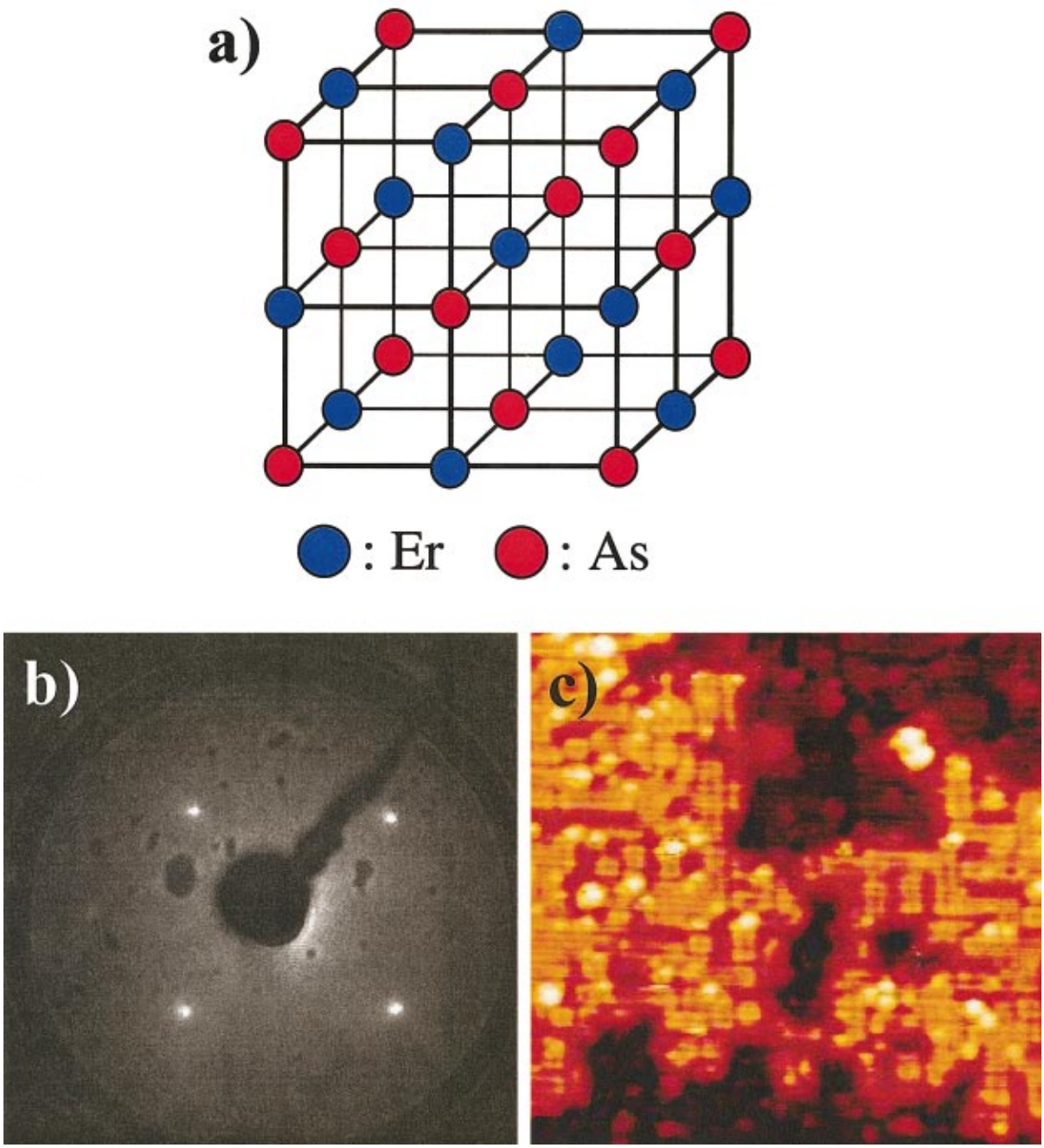

FIG. 1. (Color) The structure (a) of ErAs(100) is shown together with the LEED (b) of the stoichiometric ErAs(100) surface grown on GaAs(100) for an electron kinetic energy of 58.5 eV. The *in situ* image of STM of the growth of ErAs(100) film $(25\times25\ \text{nm})^2$ is also shown (c), and was acquired with a -2.5 V bias.

XPS intensity ratios are nearly independent of the emission angle, and in agreement with a stoichiometric ErAs as well as consistent with the known thickness of the ErAs film on the GaAs(100) substrate). The structural integrity was also confirmed by photoelectron diffraction (forward scattering), and is similar to the photoelectron diffraction effects observed for YbAs on GaAs.[27]

Angle-resolved photoemission experiments were performed at the Center for Advanced Microstructures and Devices, using the 3 meter toroidal grating monochromator (3-m TGM) beam line. The UHV chamber, used for angle-resolved photoemission, is equipped with an electron energy analyzer with an angular acceptance of $\pm1°$ and a combined (including the monochromator) energy resolution of 150 meV or better.[28] The application of symmetry and selection rules to photoemission was undertaken by comparing light incident angles of 45° ($s+p$ polarized) to 65° (more p polarized) with respect to the surface normal, making use of the highly linearly polarized light from the synchrotron as is now commonly done.[29,30]

The spin-polarized inverse photoemission experiments, using an apparatus described extensively in Refs. 14 and 31,

were undertaken in the spin-integrated mode with a transversely polarized spin electron gun based upon the Ciccacci design[32] as described elsewhere.[31] The spin electron gun was designed in a compact form in a separate chamber and the UV light (9.4 ± 0.3 eV) detected with an iodine based Geiger-Müller isochromat photon detector with a SrF_2 window. The combined inverse photoemission energy resolution was in the vicinity of 400 meV, and the wave-vector uncertainty was ± 0.025 Å^{-1} for these measurements. Typically, many experimental results were summed to improve the signal to noise ratio in spin-polarized inverse photoemission spectra.

For both photoemission and inverse photoemission, the Fermi level (E_F) was established from tantalum foils in electrical contact with the sample of ErAs(100). Conduction band features were reported with respect to this Fermi level and emission angle (or incidence angle in the case of the inverse photoemission) with respect to the surface normal. Both measurements of photoemission and inverse photoemission reported here were carried out at ambient temperatures.

The wave-vector-dependent band dispersion was investigated both parallel, $k_\parallel$, and perpendicular, $k_\perp$, to the ErAs(100) sample surface, as previously undertaken by us for other systems.[33,34] The parallel component of the wave vector ($k_\parallel$) is determined from the photoelectron (or incident electron) kinetic energy and the emission (or incidence) angle θ as

$$k_\parallel = \left(\frac{2m}{\hbar^2} E_{\mathrm{kin}} \right)^{1/2} \sin(\theta), \tag{1}$$

and $k_\parallel$ is conserved across the vacuum-solid interface.

The perpendicular component of the wave vector, $k_\perp$, is not strictly conserved across the surface-vacuum interface because of the crystal truncation. The value of $k_\perp$ can be estimated from

$$k_\perp = \left(\frac{2m}{\hbar^2} \{ E_{\mathrm{kin}} [\cos(\theta)]^2 + U_{\mathrm{in}} \} \right)^{1/2}, \tag{2}$$

where U_{in} is the inner potential, or, effectively, about the occupied bandwidth.

THEORETICAL METHODOLOGY

The general framework of our electronic structure calculations is the density functional theory[35] in the local (spin) density approximation [L(S)DA] (Ref. 36) with additional Hubbard correction terms describing electron-electron correlations associated with the narrow bands of the $4f$ electrons (LSDA+U approach[37,38]). The local-density-approximation part of the problem was treated within the linear muffin-tin orbital method[39] in the atomic sphere approximation. As is usual for non-close-packed lattices, empty spheres were introduced in the appropriate interstices.[40] The calculations were carried out scalar relativistically. The Brillouin-zone integrations were performed by the tetrahedron method[41] on a regular mesh of 1000 points in the Brillouin zone of the rocksalt lattice. These were found to be sufficient to provide results with good convergence.

It is well known that a straightforward LSDA band treatment for the $4f$'s in ErAs leads to rather poor and inadequate results,[1] because the strongly correlated $4f$ electrons cannot be adequately described within the standard LSDA framework. This is obvious because the band treatment must lead to a narrow $4f$ band at the Fermi level which strongly perturbs the rest of the band structure drastically, distorting the Fermi surface, in strong disagreement with transport measurements.[42,43] The previously used treatment of the $4f$ levels as core-like[1] is much closer to the actual situation, in which a set of narrow occupied $4f$ levels several eV below the Fermi level and a narrow set of unoccupied $4f$ states several eV above the Fermi level have only a minor effect on bands near E_F. Effectively, the treatment of the $4f$ electrons as open-shell core-like states is equivalent to the *constrained* LSDA approach of Dederichs *et al.*[44] It is also closely related to the frozen-core treatment used by Hasegawa and Yanase[4] and by Brooks and co-workers.[45,46] These approaches are somewhat controversial[34,45,46] because the $4f$ levels overlap with valence and conduction states, and the band character of the $4f$ electrons is widely recognized.[47–49]

For the purposes of this work, the treatment beyond the core-like description of the $4f$ electrons is necessary and is provided by the LSDA+U method[7,37,38] which can be viewed as a self-consistent generalization of the periodic Anderson Hamiltonian.[50] In the case of ErAs, this approach describes a narrow $4f$ band with strong Coulomb correlations that can hybridize with broad bands (e.g., Er $5d$, As $4p$), in which explicit Coulomb correlations are treated within the LSDA. Essentially, the LSDA+U approach corresponds to an unrestricted Hartree-Fock treatment of the average $4f$ electron configuration with a screened effective Coulomb energy U and an exchange energy J. As a result, the energy functional becomes orbital dependent rather than only density dependent. We use the rotationally invariant form of the LSDA+U functional,[51,52]

$$E_{\mathrm{LSDA}+U} = E_{\mathrm{LSDA}} + \frac{1}{2}(U-J) \sum_\sigma \left[\mathrm{Tr}(\rho^\sigma) - \mathrm{Tr}(\rho^\sigma \rho^\sigma) \right], \tag{3}$$

which leads to an orbital-dependent correction to the one-electron potential,

$$V_{\mathrm{LSDA}+U}(mm'\sigma) = V_{\mathrm{LSDA}} + (U-J)\left(\tfrac{1}{2} - \rho^\sigma_{mm'}\right) \tag{4}$$

where $\rho^\sigma_{mm'} = -(1/\pi)\mathrm{Im} \int^{E_F} G^\sigma_{mm'}(E) dE$ is the $4f$ orbital density matrix, and $G^\sigma_{mm'}(E)$ is the one-electron Green's function corresponding to the $4f$ orbitals m, m', and spin σ.

We emphasize that the energies U and J used in this paper are determined from the first-principle constrained LSDA calculations for a four-atom ErAs supercell and by no means are fitting parameters. In determining these parameters we followed the procedure outlined by Anisimov and Gunnarsson.[53] More precisely, we conducted total-energy calculations with different occupations of the $4f$ level treating an Er atom as an impurity in a four-atom ErAs supercell with zero intra-atomic and interatomic hopping between the $4f$ orbital and all other orbitals. The on-site Coulomb and

exchange energies can be obtained from Slater's transition state approach,[54] which leads to $U=8.6$ eV and $J=0.75$ eV. A combination of the photoemission and inverse photoemission spectra of ErAs provides an excellent opportunity to verify these values.[55,56] As we will see below, they are in a good agreement with the experiment.

Our spin-polarized calculations allow the extent of the influence of the local moments to be assessed in a material anticipated to be largely rigid band ''spin-mixed'' paramagnet, under the experimental conditions used here. It follows from our LSDA+U calculations (in agreement with previous results[1]) that in the present case the Er ion is trivalent (Er^{+3}). The ground state, therefore, is $4f^{11}$ for Er with $4f$ occupation numbers corresponding to the maximal total spin configuration, which is consistent with the first Hund's rule.[57] The existence of the localized magnetic moments resulting from the $4f$ spins in ErAs has been well established[42,43] even up to fairly elevated temperatures (e.g., well above the Néel temperature in ErAs). The magnetism in this material is thus a combination of localized magnetic moments from the open $4f$ shell and induced itinerant magnetic moments in the valence bands. The fully spin-polarized $4f$ electrons in the paramagnetic phase produce a strong spin-dependent random potential for band electrons. The electronic structure of such a disordered ''spin alloy'' could for example be calculated by means of the coherent potential approximation (CPA).[58] While this description is probably satisfactory for s and p electrons it is clearly inadequate for $4f$ states since these states are always spin-polarized ''locally'' with the ''rigid band'' exchange splitting between majority and minority states of about several eV. The spin-polarized calculations, on the other hand, treat $4f$ states properly and, therefore are suitable for the interpretation of the photoemission spectra, as indicated in Fig. 2. These calculations may be thought of as representing either a ferromagnetic phase or the saturation limit of the paramagnetic phase in a magnetic field.

The partial densities of states (PDOSs) for Er and As are presented in Fig. 3. For both sets of calculations, we have displayed the PDOSs of Er and As for majority and minority spins. The PDOSs for Er $4f$ levels in both the calculations are similar to those in experiment and show some evidence of hybridization with As (Fig. 2). The position of the occupied bands and the unoccupied $4f$ resonance in the conduction band is in good agreement with the experiment, which clearly confirms the calculated value of the Hubbard energy $U=8.6$ eV, but the absence of equivalently good agreement of the unoccupied $4f$ levels indicates strong hybridization effects. Arsenic hybridizes very strongly but only with nearest-neighbor Er atoms. This results in a large number of the Er s, p, and d states, near the Fermi level, becoming ''pulled down'' (the band binding energies increase) to the location of the As bands.

BAND SYMMETRIES AND ORBITAL HYBRIDIZATION

For ErAs(100), the photoemission spectra are dominated by three strong photoemission features, with one between E_F and about 1 eV binding energy, and another at 5 eV binding energy, as shown in Fig. 4. There are also a number of overlapping features that can be resolved between 7 and 10 eV binding energy. All of these photoemission features contain several overlapping bands, often of different symmetry.

Because of the high point group C_{4v} symmetry at the center of the surface Brillouin zone, $\bar{\Gamma}$, we can observe a number of photoemission symmetry selection rules effects. Angle-resolved photoemission spectra at the $\bar{\Gamma}$ point (normal emission) for several different photoemission geometries are compared in Fig. 4. With the surface component of the vector potential $\mathbf{A}$ ($\mathbf{A}=\mathbf{A}_\perp+\mathbf{A}_\parallel$, $\mathbf{A}_\perp$ comprises the perpendicular component of $\mathbf{A}$, and $\mathbf{A}_\parallel$ is the parallel component of $\mathbf{A}$ to the surface, respectively), which is parallel to the $\bar{\Gamma}\bar{M}$ line of the surface Brillouin zone [$\mathbf{A}_\parallel \backslash\backslash \bar{\Gamma}\bar{M}$ in Fig. 4(a)], the photoemission feature at about 1 eV binding energy is enhanced with increasing s polarization of the incident light (increasing $\mathbf{A}_\parallel$). The dominant symmetry of this band is therefore[29,30] Δ_5 (or e) containing possible contributions from orbitals of d_{zx}, d_{yz}, p_x, and p_y character. This $\bar{\Gamma}\bar{M}$ line of the surface Brillouin zone corresponds to the direction from Er to nearest-neighbor As sites (and vice versa). Given the valence configuration of erbium and arsenic, the band symmetries suggest that there are strong As $4p_x$ and $4p_y$ orbital hybridizations with Er $5d_{xz}$ and $5d_{yz}$ orbitals, respectively. This is consistent with our theoretical expectations.

With the in-plane surface component of the incident light vector potential along the $\bar{\Gamma}\bar{X}$ symmetry direction of the surface Brillouin zone, ($\mathbf{A}_\parallel \backslash\backslash \bar{\Gamma}\bar{X}$), a somewhat different light polarization dependence is observed [Fig. 4(b)]. With an increasing p polarization of the incident light (increasing $\mathbf{A}_\perp$), the photoemission feature near the Fermi level is enhanced, while, with an increasing s polarization, the photoemission feature at about 5 eV binding energy is enhanced. This light incidence angle dependence,[29,30] in this geometry, indicates that along this mirror plane of the surface, the band near E_F is of dominantly Δ_1 (or a_1) symmetry, with contributions from orbitals of s, p_z, and $d_{3z^2-r^2}$ characters, while the band at about 5 eV binding energy is now of more Δ_5 (or e) symmetry.

These results are consistent with the previous calculated band structure.[1] There are two relatively closely spaced bands of Δ_1 (or a_1) and Δ_5 (or e) symmetry along the Γ to X direction of the bulk Brillouin zone, and more recent calculations are described herein. When these bands projected onto the $\bar{\Gamma}$ point of the surface Brillouin zone, they appear to overlap. While calculations suggested that there should be spectral weights centered at about -1.5 to -2.5 and -3.5 to -4 eV of energy (binding energy) if one considers the band structure across the entire bulk Brillouin zone (Fig. 3), we find a similar (although far from identical) spectral weight density in our photoemission spectra with just the projection along $\bar{\Gamma}$. This suggests that further refinements, possibly including modified f-d and f-s hybridizations (as suggested elsewhere[34,59]) and surface and umklapp contributions, might be necessary in future band-structure calculations. Further insight into the nature of the Er-As and As-As plus Er-Er orbital hybridization is provided by the band-structure dispersion.

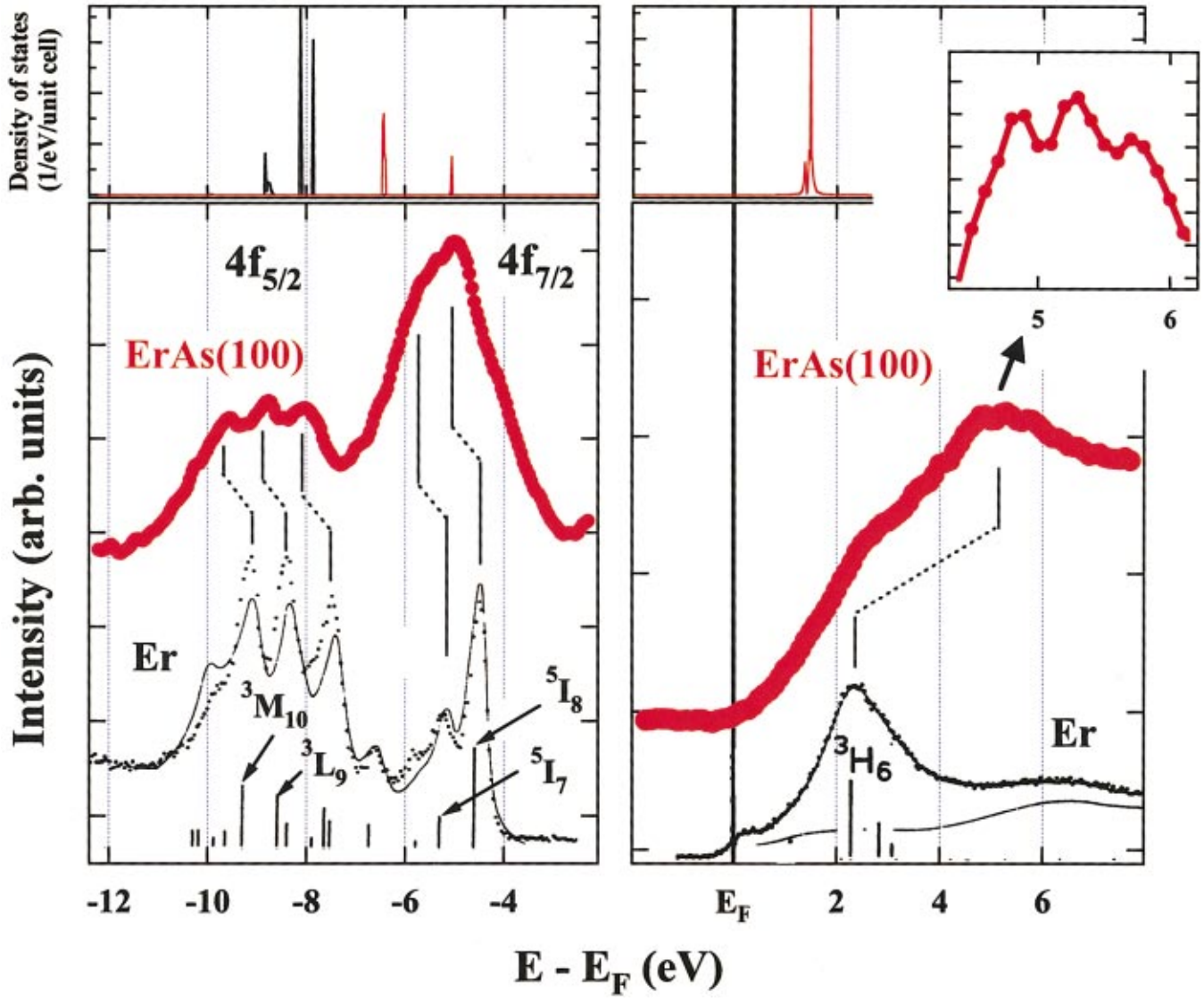

FIG. 2. (Color) Er $4f$ density of states from LSDA+U calculations of bulk ErAs (see the text). The agreement with experiment is generally fairly good for a $U=8.6$ eV. The detailed photoemission (left) and inverse photoemission (right) of the Er $4f$ multiplets for ErAs(100) grown on GaAs(100) (in red) are compared with theoretical calculations and experimental results (Ref. 55) for polycrystalline Er. The details of the unoccupied $4f$ levels are shown as an inset (an enlargement of inverse photoemission results), showing further multiplet splitting of $4f$ unoccupied states.

BAND STRUCTURE

The entire electronic band structure of ErAs(100) along the high-symmetry directions of the surface Brillouin zone $\overline{\Gamma X}$ and $\overline{\Gamma M}$ and with changing $k_\perp$ along the bulk Γ-X direction shows dispersion consistent with crystalline order and interatomic hybridization. In Fig. 5, the overlapping bands with strong Er $5d$ and $6s$ and As $4p$ contributions are indicated in the combined angle resolved photoemission and inverse photoemission spectra along the $\overline{\Gamma X}$ direction of the surface Brillouin zone. The bands near E_F exhibit a strong dispersion while the other peaks (the two overlapping peaks around -5 to -6 eV and three peaks around -7 to -10 eV) are related to the Er $4f$ multiplet levels (Fig. 2) and exhibit negligible apparent dispersion as summarized in the experimentally determined band mapping with wave vector (with changes in $k_\parallel$, the surface Brillouin zone) in Figs. 6 and 7.

To avoid any possible confusion with potential contributions from the GaAs substrate to the ErAs(100), band dispersions along the high-symmetry directions of the surface Brillouin zone were undertaken at 50 eV. At this photon energy, the GaAs states near the Fermi energy are easier to distinguish from ErAs, based on the GaAs band structure.[60] With an increasing wave vector ($k_\parallel$) parallel to the surface (increasing emission angle), the dispersion curves of ErAs(100) along $\overline{\Gamma X}$ and $\overline{\Gamma M}$ of the surface Brillouin zone are plotted in Fig. 6. The band at about 1 eV binding energy disperses rather strongly with $k_\parallel$ as well as with $k_\perp$ along the $\overline{\Gamma X}$ directing (Fig. 7). The feature at about 1.8 eV binding energy (the second band from E_F) disperses weakly with $k_\perp$ (Fig. 7) but not with $k_\parallel$ along the $\overline{\Gamma X}$ symmetry directions (Fig. 7).

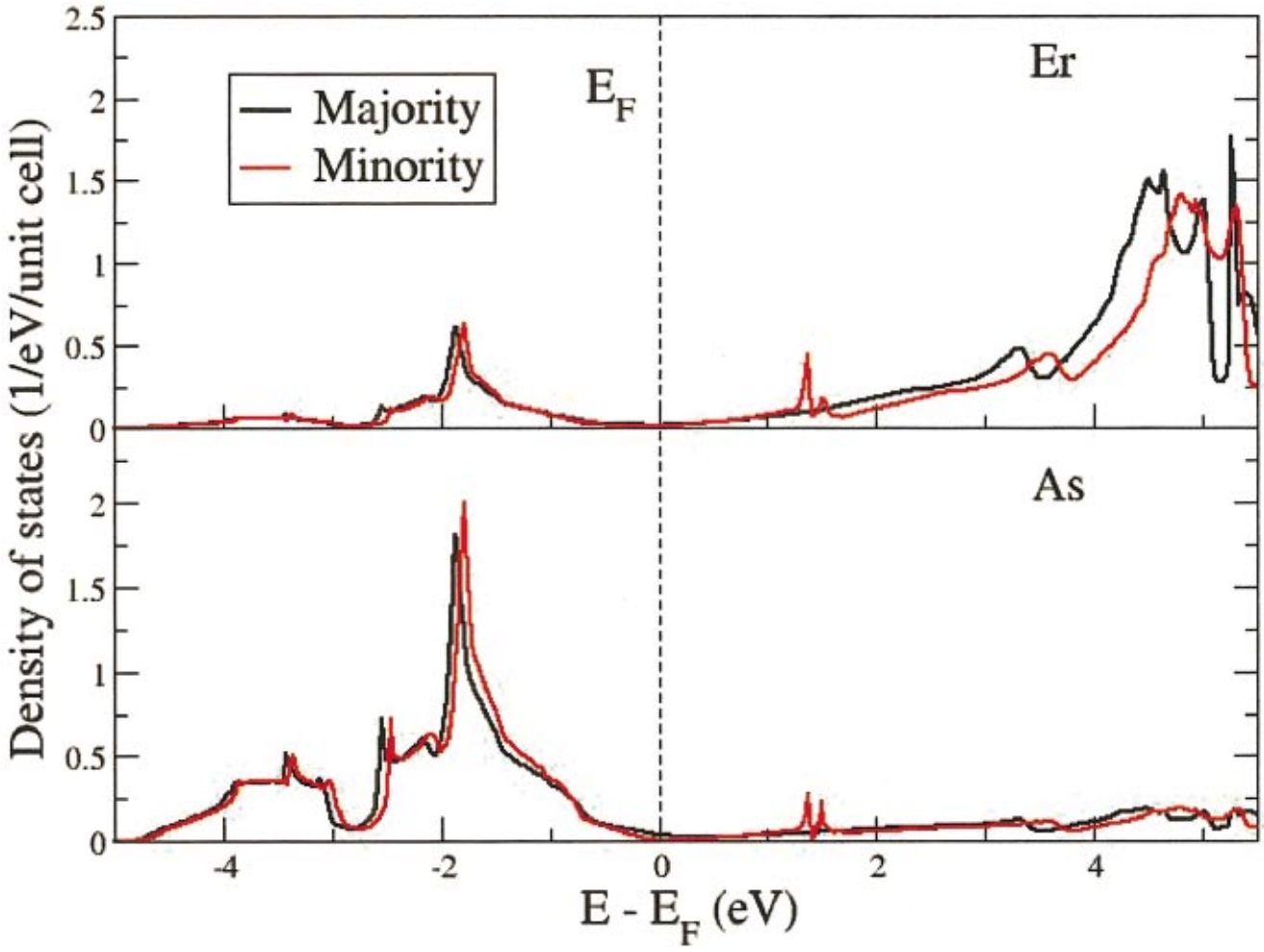

FIG. 3. (Color) The Er 5*d* density of states (a) and As density of states (b) near the Fermi energy from LSDA+U calculations of ErAs(100) (see the text). $U=8.6$ eV was used.

This suggests that this band is a surface resonance, and probably does not fall into a gap of the bulk band structure (due to the extensive dispersion of the bulk bands), as indicated in Fig. 7, and therefore it is not a true surface state. The occupied dispersing bulk band(s) must contain both Δ_1 and Δ_5 contributions that we do not resolve in this work (Fig. 5). The significant negative dispersion or dispersion toward higher binding energy from the zone center to the zone edge occurs along the $\overline{\Gamma X}$ direction of the surface Brillouin zone. Indeed, as seen in Fig. 7, both Δ_1 (or a_1) and Δ_5 (or e) symmetry bands disperse toward greater binding energies at $\overline{X}$. This suggests an in-phase relationship for the orbitals contributing to Δ_5 (or e) symmetry bands along $\overline{\Gamma X}$ (or the direction corresponding to Er to Er and As to As), and an out-of-phase relationship at $\overline{X}$. For the Δ_5 character band, this is consistent with the dominant bonding orbitals between Er and As sharing an Δ_5 (or e) symmetry, as indicated in Fig. 4(a). The increasing binding energy toward the surface Brillouin-zone edge along the $\overline{\Gamma X}$ direction of the Δ_1 (or a) symmetry band indicates that the orbitals of this symmetry are out of phase at $\overline{\Gamma}$ but partly in phase at $\overline{X}$. The Δ_1 (or a) symmetry band is therefore nonbonding or antibonding in character (the adjacent contributing atomic wave functions are out of phase at the surface Brillouin-zone center or $\overline{\Gamma}$).

The unoccupied Δ_1 (or a_1) and the Δ_5 (or e) symmetry band components also disperse toward higher binding energies with increasing $k_{\|}$ from zone center to zone edge; this occurs along the $\overline{\Gamma X}$ direction of the surface Brillouin zone, as seen in Fig. 5. In spite of the lower resolution of inverse photoemission, these bands can be resolved along both the $\overline{\Gamma X}$ and $\overline{\Gamma M}$ directions, as summarized in Fig. 6. The unoccupied band structure does exhibit a qualitative agreement with the bulk band structure,[1–3,18] but the splitting at $\overline{\Gamma}$, between Δ_1 (or a_1) and the Δ_5 (or e) symmetry bands, is far larger than the 80 meV splitting (since it is resolvable at two unoccupied bands) predicted to occur at the Γ point of the bulk band structure.[1,18] This is possibly because in the isochromat mode of inverse photoemission one may be off the Γ point of the bulk band structure. The angle-resolved inverse photoemission is very surface sensitive, and cannot be exploited to probe only the bulk band structure in our apparatus, but does suggest the possibility of a Fermi level crossing along $\overline{\Gamma X}$ of the surface Brillouin zone, as indicated in Fig. 5, and plotted in Figs. 6 and 7. The first band at about 1.6 eV

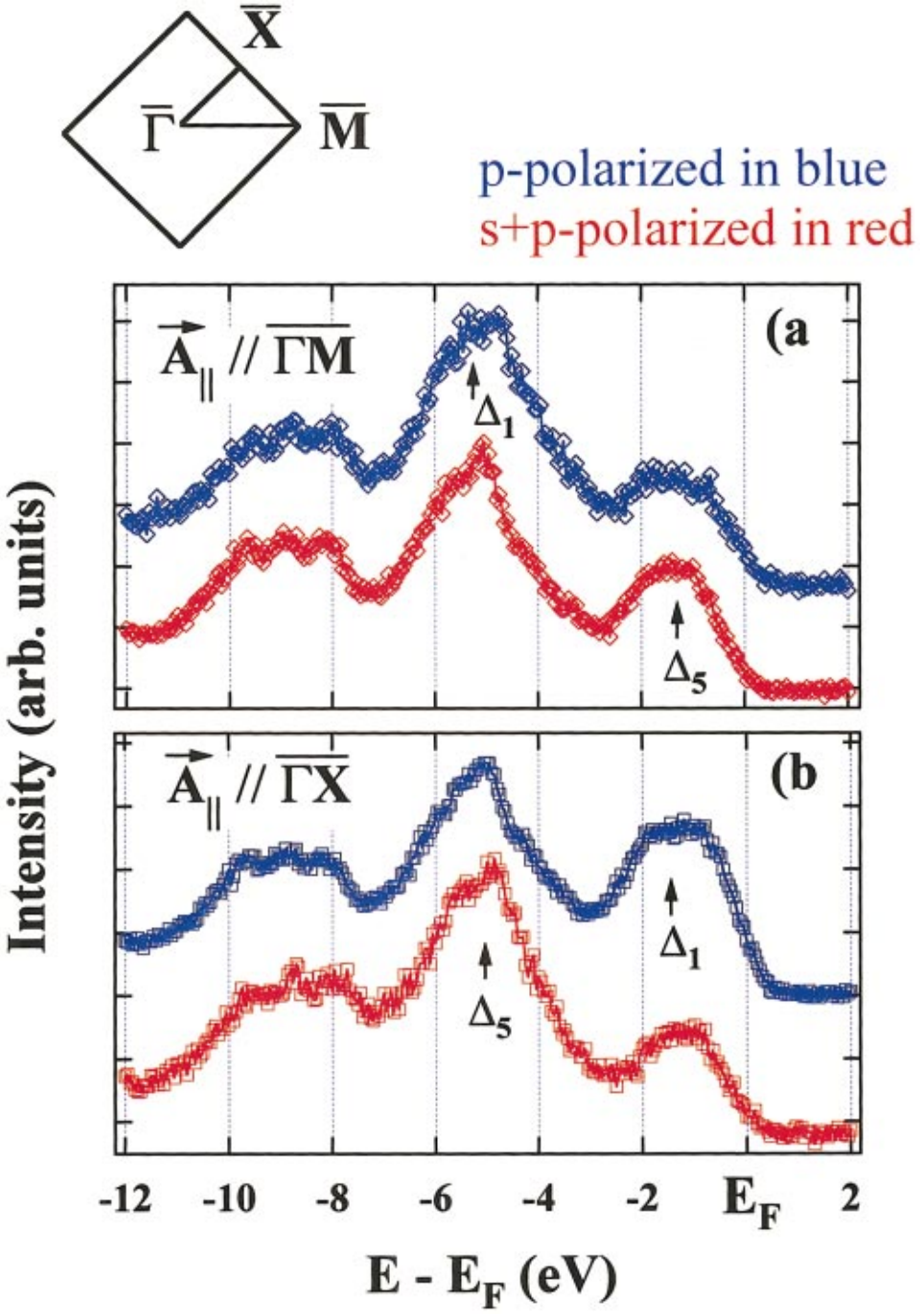

FIG. 4. (Color) Normal-emission photoemission spectra of epitaxial ErAs(100) grown on GaAs(100) in different light polarization geometries for a 50 eV photon energy. The spectra were taken with the component of $\mathbf{A}_{\|}$ parallel with the surface along different mirror planes of the surface Brillouin zone, i.e., the $\overline{\Gamma M}$ direction, $\mathbf{A}_{\|}\backslash\backslash\overline{\Gamma M}$ (a) and $\overline{\Gamma X}$ $\mathbf{A}_{\|}\backslash\backslash\overline{\Gamma X}$ (b). For each mirror plane geometry, two different light incidence angles or orientations of the polarization vector with respect to the surface normal are shown: 65° or largely *p*-polarized light (**A** is relatively normal to the sample surface) in blue, and 45° or $(s+p)$-polarized light in red. The Δ_5 (or *e*) and the Δ_1 (or a_1) symmetry bands are indicated with arrows as appropriate. The schematic of the surface Brillouin zone of the crystal is an inset at the top of the figure.

above E_F does disperse toward the Fermi level with increasing wave vector, in good agreement with our theoretical expectations plotted in Fig. 9. From the density of states, near the Fermi level, obtained in inverse photoemission, we identify an unoccupied band crossing of the Fermi level at about 0.4 Å^{-1} along the $\overline{\Gamma X}$ direction of the surface Brillouin zone (not seen in the angle resolved photoemission), as indicated in the intensity plot in Fig. 7. In spite of the fact that the band dispersion is larger than expected in photoemission, in general, the negligible density of states at the Fermi level in inverse photoemission suggests that the surface is far less metallic than the near-surface region or bulk material. The correlation energy, therefore, must be greater at the surface than in the bulk. It was already noted[61] that the surface of ErAs(100) exhibits large surface to bulk core-level shifts of about 1.1 eV and a low effective surface Debye temperature. These are further indications that the surface has a different electronic structure from the bulk, possibly related to a surface relaxation, discussed in detail elsewhere.[61]

Figure 8 shows the photon energy dependence of the overlapping Δ_1 (or *a*) and Δ_5 (or *e*) peaks near to E_F, in the angle-resolved photoemission spectra. There is a shift of the photoemission feature binding energy toward E_F and a diminution of intensity as the photon energy is increased from 45 eV to about 60 eV photon energy followed by an increase in photoemission intensity and binding energy with a contin-

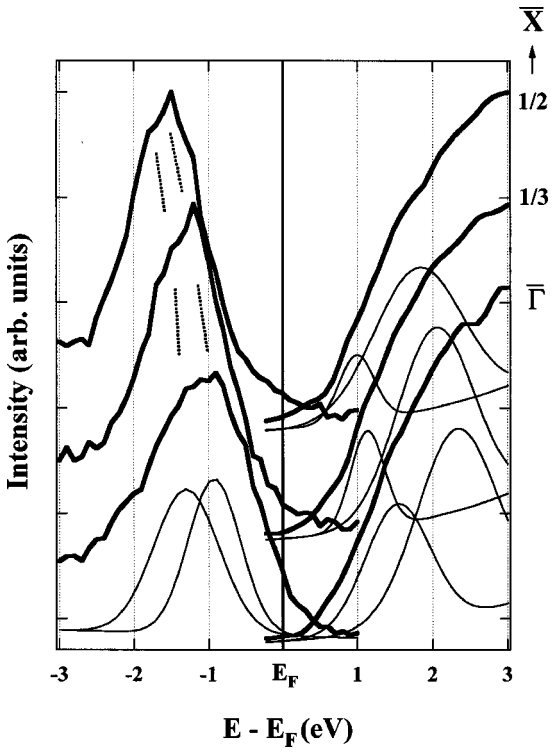

FIG. 5. The combined angle-resolved photoemission (left) and inverse photoemission (right) along the $\overline{\Gamma X}$ symmetry line of surface Brillouin zone. The peak positions and possible dispersion are indicated for these bands closest to the Fermi energy. There are two occupied bands in photoemission, as is indicated by a possible fitting to the photoemission data, and suggested by the light polarization dependence, but are not easily resolved.

ued increase in photon energy from 60 to 80 eV. These concomitant changes in the band dispersion and intensity changes are summarized in Fig. 7. These changes in binding energy and photoemission intensity can be understood as indicative of a Fermi-level crossing, as suggested by the earlier band-structure calculations,[1–3] and those described later. Schematically, to illustrate the effect of a Fermi-level crossing, we have superimposed peak fittings to each spectrum as a function of photon energy, shown in Fig. 8. These results are consistent with the Fermi-level crossing identified in inverse photoemission across the surface Brillouin zone.

These binding energy and intensity changes along $\overline{\Gamma X}$ symmetry lines of surface Brillouin zone are compared with the band structure along $k_\perp$ (the bulk band structure) in Fig. 7. There are few changes in the photoemission intensity along the $\overline{\Gamma X}$ direction of the surface Brillouin zone, though there is a significant dispersion of the band(s). On the other hand, along Γ to X of the bulk Brillouin zone, in photoemission, and along the $\overline{\Gamma X}$ direction of the surface Brillouin zone, in inverse photoemission, there are significant changes in intensity as well as even more significant band dispersions. The dramatic change in the photoemission intensity of the Δ_1 (or a) and Δ_5 (or e) symmetry bands is a vivid indicator of the E_F crossing of the valence bands with changing k-perpendicular values. By taking intensity changes into account, we assert that the band dispersion along the k-perpendicular (directory along Γ to X) is more significant than indicated by binding energy along $\overline{\Gamma X}$, as alluded to above and as we summarize in Fig. 7.

This result for the bulk band structure shows a good qualitative agreement with the theoretical band-structure calculations,[1–3] and our recent calculations plotted in Fig. 9. However, the extent of the experimental band dispersion is still smaller than that calculated for the Δ_1 (or a) along Γ to X of the bulk Brillouin zone by about $\frac{1}{2}$, and much smaller than the dispersion expected from band structure theory along Γ to L of the bulk Brillouin zone. A simple admixture from Δ_5 would bring the experiment into greater consistency with the calculation, as the band dispersion calculated for the

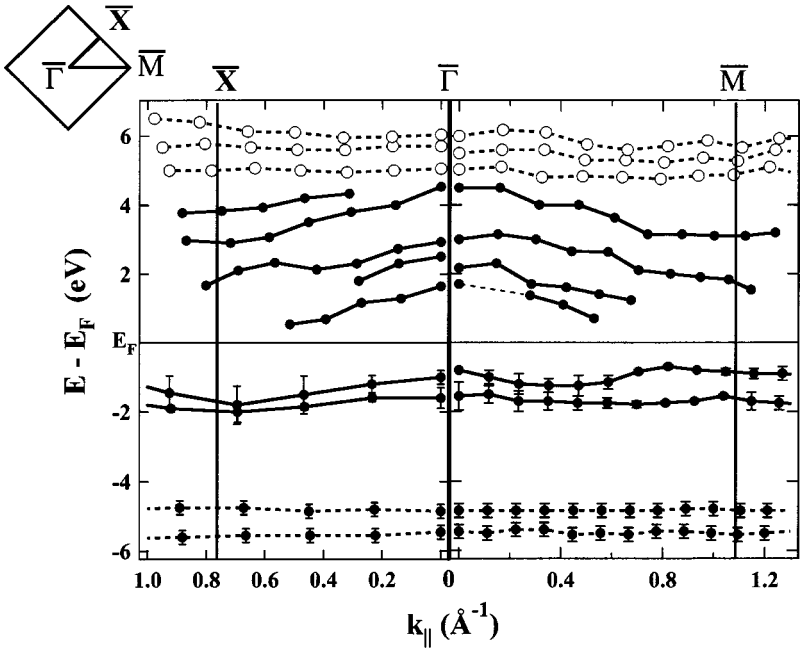

FIG. 6. The experimental band structure of the ErAs(100), along $\overline{\Gamma X}$ and $\overline{\Gamma M}$ high-symmetry lines of the surface Brillouin zone compiled from combined photoemission (bottom) and inverse photoemission (top) results. The high-symmetry points and directions of the surface Brillouin zone of the crystal is indicated in the inset at the top of the figure. Bands with a strong $4f$ weight are indicated by the dashed lines.

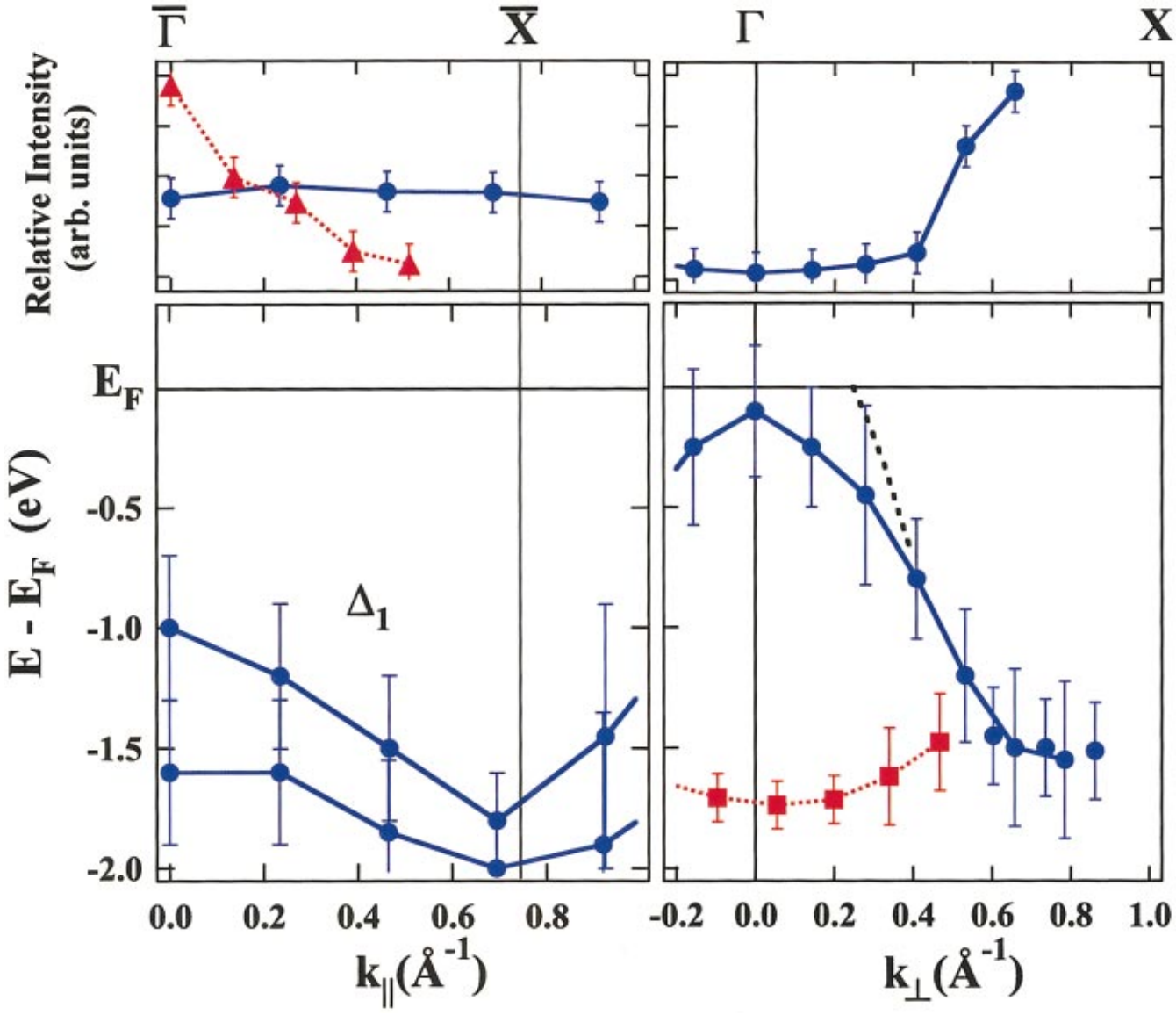

FIG. 7. (Color) The bulk band dispersion along Γ to *X* (normal emission, but changing photon energy) compared to the dispersion along $\overline{\Gamma X}$ (50 eV photon energy but changing emission angle) of the surface Brillouin zone. This compares the $k_{\|}$ (left) with $k_{\perp}$ (right) dependent dispersion of the highly dispersive band(s) near E_F. The surface resonance can be identified near the Brillouin-zone center by a dispersion that is largely independent of photon energy (the dashed line and square symbols in red along Γ to *X*). The intensity changes, with the wave vector, of the occupied band(s) closest to the Fermi level are indicated. This suggests a Fermi level crossing of this band, along the Γ to *X* direction of the bulk band structure, as indicated by the dashed black line. The data are summarized from spectra like those shown in Fig. 8. A Fermi-level crossing along $\overline{\Gamma X}$ is suggested by the intensity plots, near E_F, from inverse photoemission (red) but not in photoemission at 50 eV (blue).

Δ_1 band is one-half that of experiment, but even without a clear resolution of the Δ_5 bulk band it is clear that this band disperses more in the experiment than predicted by theory.

We do not see a clear separation of the Δ_1 and Δ_5 bands resolved at $k_{\perp}$ values well away from the bulk Brillouin zone Γ point, as would be expected from theory, except in inverse photoemission. Further, the data in Fig. 8 (along Γ to *X*) are taken with *p*-polarized light that should suppress the Δ_5 band. In the previous study of the experimental band structure of ErAs(100),[24] the unexpectedly small surface band dispersion and the absence of bulk band dispersion (no dispersion with changing photon energy) were attributed to the two-dimensional character of an epitaxial ErAs(100) surface grown on GaAs(100). Our films are similar in thickness to those discussed in that previous work, yet we have observed bulk band dispersion. Obviously, other considerations may have to be considered, such as the necessity for single-phase materials and possible contributions from strain and strain-induced dislocations.

There is good agreement between the binding energies of the $4f$ levels in experiment and theory, with the calculated correlation energy of 8.6 eV. As noted previously, the ab-

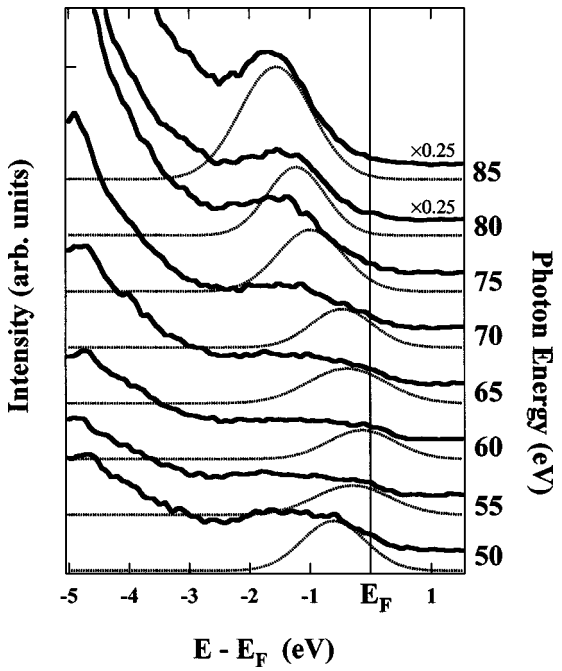

FIG. 8. Photon energy dependence of the photoemission along Γ to *X*. The data was taken with *p*-polarized light and normal emission.

sence of any significant dispersion of any of the occupied or unoccupied $4f$ multiplet states, as plotted by the dashed lines in Fig. 6, is consistent with the expected dispersion of these levels in the calculated band structure (Fig. 9). Since the

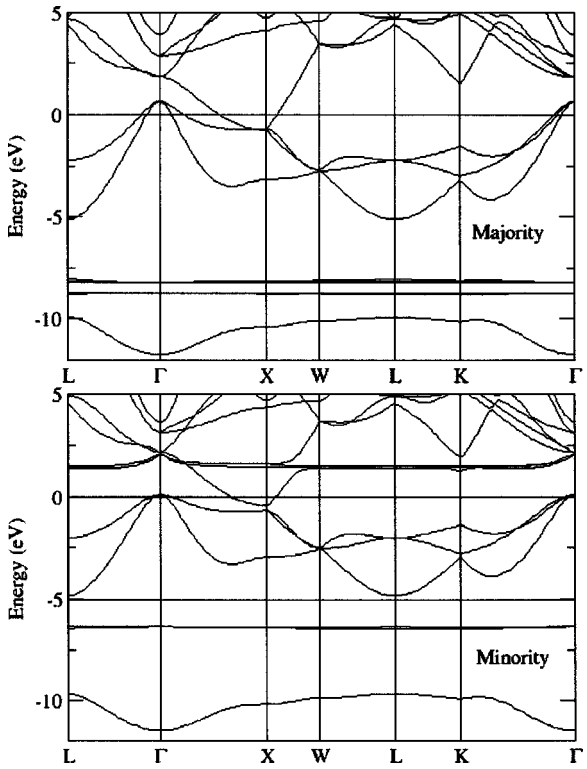

FIG. 9. The calculated LSDA+U band structure of ErAs for majority (top panel) and minority spins (lower panel).

value of the Hubbard U is finite, although large ($U = 8.6$ eV), this does suggest some hybridization between the Er $4f$ and Er $5d$ levels. The very localized nature of the $4f$ electrons is a result of the high centrifugal "barrier" $l(l+1)/r^2$ for the $4f$ states. Thus, in spite of the fact that their energetic positions overlap with the broad bands of the system, these levels form very narrow resonances. In the case of the uranium $5f$ levels and the $4f$ levels in $CeSb_2$, where $5f/4f$ level dispersion was observed experimentally,[62,63] this suggests a smaller f level localization (greater delocalization) than occurs for ErAs(100) or Gd(0001).[34]

MULTIPLET STRUCTURES

The multiplet structure of Er $4f$ levels in ErAs(100), grown on GaAs(100), is clearly evident in Fig. 2. Such $4f$ multiplet splittings for Er metal[55] and erbium silicides[64] have been reported. Er $4f$ multiplet splittings of epitaxial ErAs(100) grown on GaAs(100) can be compared to the theoretical[55,65] and experimental[55] multiplet splittings of Er metal. Figure 2 shows the experimental results for ErAs(100) (upper experimental spectra in red) and theoretical and experimental calculations of Er metal cited in Ref. 55. With shifts of about 0.5 eV toward increasing binding energy for the occupied $4f$ multiplets (seen in photoemission below E_F in Fig. 2), and shifts of about 3 eV away from E_F for the unoccupied $4f$ levels (seen as inverse photoemission above E_F in Fig. 2), we can align the $4f$ multiplets observed with ErAs with those of Er metal.

The increase in the energy difference of $4f$ orbitals between occupied and unoccupied suggests strong chemical shifts and crystal-field effects[66] but the large shift away from the Fermi level for the unoccupied $4f$ levels of ErAs relative to the smaller shift away from the Fermi level by the occupied $4f$ levels cannot be entirely explained by the differences in occupied and unoccupied $4f$ populations. Final-state effects in photoemission, and inverse photoemission[67] cannot, *a priori*, be excluded. This is particularly true as it appears that the surface layer electronic structure tends toward that of a *p*-type semiconductor, as noted in the discussion of the band structure above. Final-state effects, therefore, may affect inverse photoemission to a greater extent than photoemission.

CONCLUSIONS

The rare-earth pnictides ErAs(100), group-V compounds grown epitaxially on GaAs(100), show sufficient crystalline order to exhibit band dispersion. Combining the experimental band mappings and photoemission selection rules, we assign the surface resonance and bulk bands of ErAs(100). Through a combination of photoemission and inverse photoemission spectroscopy, and changes in spectral weight, we have band dispersion with the wave vector parallel ($k_\parallel$) and perpendicular ($k_\perp$) to the sample surface. The experimental band dispersion is qualitatively similar to that of theoretical calculations, but the extent of the dispersion is far smaller

than expected from theory. The Δ_1 (or a_1) and Δ_5 (or e) symmetry characters of the bands nearest to the Fermi level (E_F) are seen to cross E_F in the bulk band structure, but further study is clearly indicated to assess the all important relative weights of Er and As as a function of the wave vector.

ACKNOWLEDGMENTS

This work was supported by NSF through Grant Nos. DMR-98-02126 and DMR-0071823, the Center for Materials Research and Analysis (CMRA), and the Office of Naval Research.

[1] A. G. Petukhov, W. R. L. Lambrecht, and B. Segall, Phys. Rev. B **53**, 4324 (1996).
[2] A. G. Petukhov, W. R. L. Lambrecht, and B. Segall, Phys. Rev. B **50**, 7800 (1994).
[3] W. R. L. Lambrecht, B. Segall, A. G. Petukhov, R. Bogaerts, and F. Herlach, Phys. Rev. B **55**, 9239 (1997).
[4] Akira Hasegawa and Akira Yanase, J. Phys. Soc. Jpn. **42**, 492 (1977).
[5] A. Hasegawa, J. Phys. C **13**, 6147 (1980); J. Phys. Soc. Jpn. **54**, 677 (1985).
[6] C. Stampfl, W. Mannstradt, R. Asahi, and A. J. Freeman, Phys. Rev. B **63**, 155106 (2001).
[7] A. I. Liechtenstein, V. P. Antropov, and B. N. Harmon, Phys. Rev. B **49**, 10 770 (1994).
[8] G. Travaglini, F. Marabelli, R. Monnier, E. Kaldis, and P. Wachter, Phys. Rev. B **34**, 3876 (1986).
[9] R. Monnier, J. Rhyner, T. M. Rice, and D. D. Koelling, Phys. Rev. B **31**, 5554 (1985).
[10] Jian-Bai Xia, Shang-Fen Ren, and Yia-Chung Chang, Phys. Rev. B **43**, 1692 (1991).
[11] D. X. Li, Y. Haga, H. Shida, T. Suzuki, Y. S. Kwon, and S. Kido, J. Phys.: Condens. Matter **9**, 10 777 (1997).
[12] H. R. Child, M. K. Wilkinson, J. W. Cable, W. C. Koehler, and E. Wollan, Phys. Rev. **131**, 922 (1963).
[13] G. Busch, J. Appl. Phys. **38**, 1386 (1967).
[14] C. Waldfried, T. McAvoy, D. Welipitiya, Takashi Komesu, P. A. Dowben, and E. Vescovo, Phys. Rev. B **58**, 7434 (1998).
[15] Takashi Komesu, C. Waldfried, and P. A. Dowben, Phys. Lett. A **256**, 81 (1999).
[16] D. E. Brehmer, K. Zhang, C. J. Schwarz, S. P. Chau, and S. J. Allen, Appl. Phys. Lett. **67**, 1268 (1995).
[17] D. E. Brehmer, K. Zhang, C. J. Schwartz, S. P. Chau, S. J. Allen, J. P. Ibbetson, A. G. Petukhov, C. J. Palmstrøm, and B. Wilkens, Solid-State Electron. **40**, 241 (1996).
[18] A. G. Petukhov, W. R. L. Lambrecht, and B. Segall, Phys. Rev. B **53**, 3646 (1996).
[19] Ph. Mavropoulos, N. Papanikolaou, and P. H. Dederichs, Phys. Rev. Lett. **85**, 1088 (2000).
[20] B. C. Lee and Y. C. Chang, Phys. Rev. B **51**, 316 (1995).
[21] J. M. MacLaren, X.-G. Zhang, W. H. Butler, and X. Wang, Phys. Rev. B **59**, 5470 (1999).
[22] L. Degiorgi, W. Bacsa, and P. Wachter, Phys. Rev. B **42**, 530 (1990).
[23] Hajime Yamada, Tadashi Fukawa, Takayuki Muro, Yoshiki Tanaka, Shin Imada, Shigemasa Suga, D.-X. Li, and Takashi Suzuki, J. Phys. Soc. Jpn. **65**, 1000 (1996).
[24] L. Ilver, J. Kanski, C. Wigren, U. O. Karlsson, and P. R. Varekamp, Phys. Rev. Lett. **77**, 4946 (1996).
[25] C. G. Olson, P. J. Benning, M. Schmidt, D. W. Lynch, P. Canfield, and D. M. Wieliczka, Phys. Rev. Lett. **76**, 4265 (1996).
[26] C. J. Palmstrøm, N. Tabatabaie, and S. J. Allen, Jr., Appl. Phys. Lett. **53**, 2608 (1988).
[27] B. Lepine, A. Quemerais, D. Sebilleau, G. Jezequel, D. Agliz, Y. Ballini, and Guivarc'h, J. Appl. Phys. **76**, 5218 (1994).
[28] P. A. Dowben, D. LaGraffe, and M. Onellion, J. Phys.: Condens. Matter **1**, 6571 (1989).
[29] E. W. Plummer and W. Eberhardt, Adv. Chem. Phys. **49**, 533 (1982), W. Eberhardt and E. W. Plummer, Phys. Rev. B **21**, 3245 (1980).
[30] J. Hermanson, Solid State Commun. **22**, 9 (1977); M. Scheffler, K. Kambe, and F. Forstmann, *ibid.* **25**, 93 (1978).
[31] Takashi Komesu, C. Waldfried, Hae-Kyung Jeong, D. P. Pappas, T. Rammer, M. E. Johnston, T. J. Gay, and P. A. Dowben, Proc. SPIE **3945**, 6 (2000).
[32] F. Ciccacci, E. Vescovo, G. Chiaia, S. De Rossi, and M. Tosca, Rev. Sci. Instrum. **63**, 3333 (1992).
[33] I. N. Yakovkin, Jiandi Zhang, and P. A. Dowben, Phys. Rev. B **63**, 115408 (2001).
[34] I. N. Yakovkin, Takashi Komesu, and P. A. Dowben, Phys. Rev. B **66**, 035406 (2002).
[35] P. Hohenberg and W. Kohn, Phys. Rev. B **136**, B864 (1964); W. Kohn and L. J. Sham, *ibid.* **140**, A1133 (1965).
[36] U. von Barth and L. Hedin, J. Phys. C **5**, 1629 (1972).
[37] V. I. Anisimov, J. Zaanen, and O. K. Andersen, Phys. Rev. B **44**, 943 (1991).
[38] V. I. Anisimov, I. V. Solovyev, M. A. Korotin, M. T. Czyzyk, and G. A. Sawatzky, Phys. Rev. B **48**, 16 929 (1993).
[39] O. K. Andersen, O. Jepsen, and M. Sob, in *Electronic Band Structure and its Applications*, edited by M. Yussouff (Springer, Heidelberg, 1987), p. 1.
[40] D. Gloetzel, B. Segall, and O. K. Andersen, Solid State Commun. **36**, 403 (1980).
[41] O. Jepsen and O. K. Andersen, Solid State Commun. **9**, 1763 (1971); P. E. Bloechl, O. Jepsen, and O. K. Andersen, Phys. Rev. B **49**, 16 223 (1994).
[42] S. J. Allen, Jr., N. Tabatabaje, C. J. Palmstrøm, G. W. Hull, T. Sands, F. DeRosa, H. L. Gilchrist, Phys. Rev. Lett. **62**, 2309 (1989).
[43] S. J. Allen, Jr., F. DeRosa, C. J. Palmstrøm, and A. Zrenner, Phys. Rev. B **43**, 9599 (1991).
[44] P. H. Dederichs, S. Blugel, R. Zeller, and H. Akai, Phys. Rev. Lett. **53**, 2512 (1984).
[45] M. S. S. Brooks, L. Nordstrom, and B. Johansson, J. Phys.: Condens. Matter **3**, 2357 (1991).
[46] R. Ahuja, S. Auluck, B. Johansson, and M. S. S. Brooks, Phys. Rev. B **50**, 5147 (1994).
[47] W. M. Temmerman and P. A. Sterne, J. Phys. C **2**, 5529 (1990).
[48] D. J. Singh, Phys. Rev. B **44**, 7451 (1991).
[49] M. Heinemann and W. M. Temmerman, Phys. Rev. B **49**, 4348 (1994).

[50] P. W. Anderson, Phys. Rev. **124**, 41 (1961).
[51] S. L. Dudarev *et al.*, Phys. Rev. B **57**, 1505 (1998).
[52] A. I. Liechtenstein, V. I. Anisimov, and J. Zaanen, Phys. Rev. B **52**, R5467 (1996).
[53] V. I. Anisimov and O. Gunnarsson, Phys. Rev. B **43**, 7570 (1991).
[54] J. C. Slater, *The Self-Consistent Field for Molecules and Solids* (McGraw-Hill, New York, 1974), Vol. 4, p. 35.
[55] J. K. Lang, Y. Baer, and P. A. Cox, J. Phys. F: Met. Phys. **11**, 121 (1981).
[56] J. F. Herbst, D. N. Lowy, and R. E. Watson, Phys. Rev. B **6**, 1913 (1972).
[57] F. Hulliger, in *Handbook on the Physics and Chemistry of Rare Earths*, edited by K. A. Gshneidner and L. Eyring (North-Holland, Amsterdam, 1979), Vol. 4, p. 153.
[58] T. Moriya, J. Magn. Magn. Mater. **14**, 1 (1979).
[59] P. Strange, A. Svane, W. M. Temmerman, Z. Szotek, and H. Winter, Nature (London) **399**, 756 (1999).
[60] Y. Q. Cai, A. P. J. Stampfl, J. D. Riley, R. C. G. Leckey, B. Usher, and L. Ley, Phys. Rev. B **46**, 6891 (1992).
[61] H. K. Jeong, Takashi Komesu, P. A. Dowben, B. D. Schultz, and C. J. Palmstrøm, Phys. Lett. A **302**, 217 (2002).
[62] C. G. Olson, S. J. Chase, P. Canfield, and D. W. Lynch, J. Electron Spectrosc. Relat. Phenom. **93**, 175 (1998).
[63] A. B. Andrews, J. J. Joyce, A. J. Arko, J. D. Thompson, J. Tang, J. M. Lawrence, and J. C. Hemminger, Phys. Rev. B **51**, R3277 (1995).
[64] L. Stauffer, C. Pirri, P. Wetzel, A. Mharchi, P. Paki, D. Bolmont, G. Gewinner, and C. Minot, Phys. Rev. B **46**, 13 201 (1992).
[65] F. Gerken, J. Phys. F: Met. Phys. **13**, 703 (1983).
[66] Stefan Hüfner, in *Photoelectron Spectroscopy*, edited by Manuel Cardona, Springer Series. in Solid-State Science Vol. 82 (Springer, New York 1995).
[67] J. E. Ortega, F. J. Himpsel, Dongqi Li, and P. A. Dowben, Solid State Commun. **91**, 807 (1994).